

Article Type

Fluid and kinetic modelling for non-local heat transport in magnetic fusion devices

Guido Ciralo*,¹ Hugo Bufferand,¹ Pierfrancesco Di Cintio,^{2,3} Philippe Ghendrih,¹ Stefano Lepri,^{4,3} Roberto Livi,^{5,3,4} Yannick Marandet,⁶ Eric Serre,⁷ Patrick Tamain,¹ and Matteo Valentinuzzi¹

¹*IRFM, CEA, F-13108 St Paul Lez Durance, France*

²*IFAC, CNR, I-50019 Sesto Fiorentino, Italy*

³*INFN, Sezione Firenze, I-50019 Sesto Fiorentino, Italy*

⁴*ISC, CNR, I-50019 Sesto Fiorentino, Italy*

⁵*Dipartimento di Fisica e Astronomia and CSDC, Università di Firenze, I-50019 Sesto Fiorentino, Italy*

⁶*PIIM, CNRS - Aix-Marseille Université, F-13397 Marseille, France*

⁷*M2P2, CNRS - Aix-Marseille Université, F-13451 Marseille, France*

Correspondence: *Guido Ciralo, CEA IRFM, 13108 St Paul Lez Durance. Email: guido.ciralo@cea.fr

Received 00 XXX 0000; Revised 00 XXX 0000; Accepted 00 XXX 0000

Summary

In order to improve the presently used ad hoc flux limiter treatment of parallel heat flux transport in edge plasma fluid codes we consider here a generalized version of the Fourier law implementing a non-local kernel for the heat flux computation. The Bohm boundary condition at the wall is recovered introducing a volumetric loss term representing the contribution of suprathermal particles to the energy out flux. As expected, this contribution is negligible in the strongly collisional regime while it becomes more and more dominant for marginally and low collisional regimes. In the second part of the paper, we consider a kinetic approach where collisions are considered using the Multi-Particle-Collision (MPC) algorithm. Kinetic simulation results at medium and low collisionality are also reported.

Keywords: Heat transport, Coulomb collisions, Kinetic equations, Fluid models

1 Introduction

Modelling parallel heat transport in edge tokamak plasma is a crucial issue for predictions of power loads on divertor targets. In the operational regimes of interest for a magnetic fusion device a significant temperature gradient will build up along the field line between the upstream hot region that acts as a heat source, and the colder plasma region at the wall that acts as a sink. Numerical estimations of edge and SOL plasma rely mainly on 2D transport codes

like e.g. SOLEDGE2D [1], SOLPS-ITER[2], EDGE2D [3], SONIC[4], UEDGE[5]. These numerical tools are based on a fluid approach and a collisional closure with the so-called Spitzer-Härm (hereafter SH, see Ref. [6]) expression for the parallel heat flux

$$q_{\parallel}(x) = -\kappa(x)\nabla_{\parallel}T(x), \quad (1)$$

where the thermal conductivity $\kappa(x)$ is computed in the strong collisionality assumption (i.e. considering a small departure from the Maxwellian distribution function), and reads

$$\kappa(x) = \kappa_0 T(x)^{5/2}. \quad (2)$$

When collisionality drops, the classical Fourier law fails in describing heat transport, and the expression above leads to overestimated heat fluxes (see e.g [7, 8] and references therein).

Typically, in order to avoid unphysical divergences in the SH expression for the heat flux, an *ad hoc* flux limiter correction is introduced with the following harmonic average between the free streaming heat flux $q_{FS} = nv_{th}T$ and the collisional expression q_{SH} :

$$q_{\parallel} = \left(\frac{1}{q_{SH}} + \frac{1}{\alpha n v_{th} T} \right)^{-1}. \quad (3)$$

In the formulae above v_{th} is the thermal velocity, n the plasma density and α is a free parameter ranging from 0.1 to 3 characteristic values.

In Figure 2 we report an example of the strong impact that such flux limiter expression can have on the predictions obtained from transport codes on energy fluxes at the wall. We consider a SOLEDGE2D simulation for WEST configuration [9] in pure Deuterium with an input power $P_{in} = 4MW$ and a gas puff activated in the private flux region with an injection rate equal to 4×10^{21} atoms per second. The radial transport coefficients D for density, χ_i for ion temperature and χ_e for electron temperature are reported in Fig.1. They are settled equal to the ones presented in [10] and, waiting for measurements on WEST plasmas, have been chosen taking into account parameters which have been adjusted to match experimental mid-plane profiles of a H-mode ASDEX Upgrade plasma (see Ref. [11]). The SOLEDGE-EIRENE simulations are performed considering three different expressions for the electron heat flux transport (while the ion heat flux is always computed using the flux limiter expression with $\alpha = 0.2$): in the first simulation we do not activate the flux limiters (FL) and the electron heat flux is computed using the SH expression. In the second and third simulations the electron heat flux is computed using the flux limiter expression given by Eq.(3) with $\alpha = 0.3$ and $\alpha = 0.15$, respectively. In Figure 2 (panel a), we show with a 2D colour map the electron temperature in a WEST poloidal section obtained in the SH case. The comparison between the electron

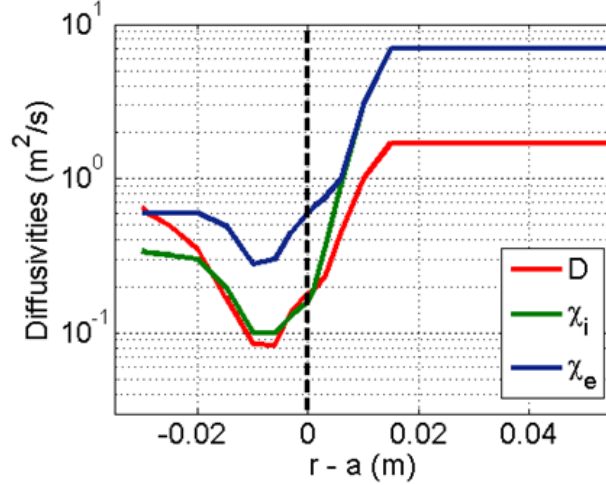


Figure 1: Radial profiles of flux surface averaged transport coefficients used in SOLEDGE2D-EIRENE simulations inspired from Ref.^[11]

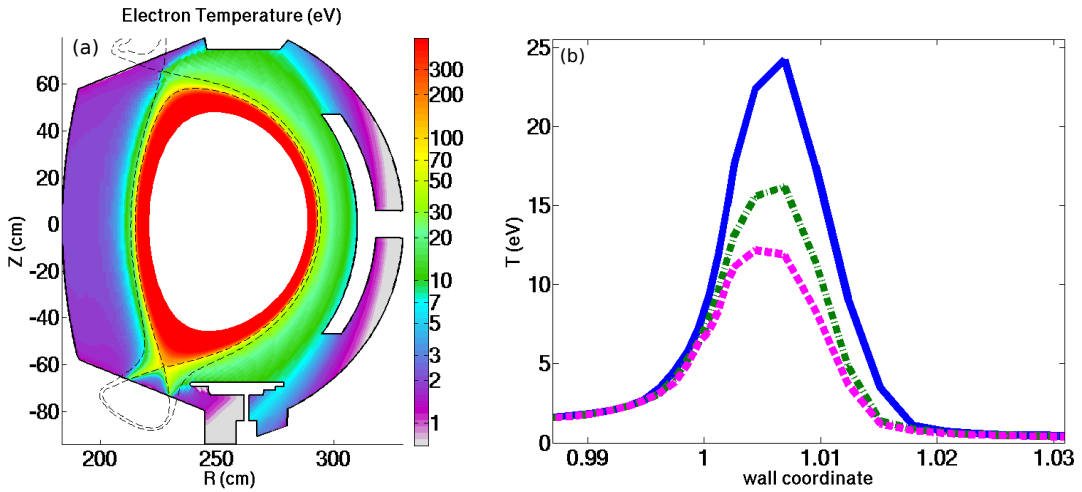


Figure 2: Contour plot of the electron temperature in the poloidal section obtained from a SOLEDGE2D-EIRENE simulation (using the SH expression for the electron heat flux computation) with input power $P_{in} = 4MW$ and a gas puff of 4×10^{21} atoms per second activated in the private flux region (a). Electron temperature profiles on the outer divertor target computed using SH expression (solid blue line), flux limiter expressions with parameter $\alpha = 0.3$ (dash-dot green line), and $\alpha = 0.15$ (dashed pink line) (b).

temperature profiles at the outer strike point obtained from these three different cases (SH, FL with $\alpha = 0.3$ and FL with $\alpha = 0.15$) is presented in panel (b). We note that there is a strong reduction of the temperature peak value between the SH case and the one computed with a FL equals to $\alpha = 0.15$.

In order to improve the presently used ad hoc flux limiter treatment of parallel heat flux transport in edge plasma codes we consider a fluid description with the generalized version of the Fourier law implementing a non-local kernel

for the heat flux computation as proposed, for example, in the paper by Luciani and co-authors ^[24]

$$q_{NL}(x) = - \int w(x, x') \kappa(x') \nabla T(x') dx', \quad (4)$$

where q_{NL} is the *non-local* heat flux, w the delocalization kernel, κ the classical Spitzer-Härm collisional conductivity and T the temperature. The simplest phenomenological form of the kernel is the one in which memory decays exponentially in space,

$$w(x, x') = \frac{1}{2\lambda(x')} \exp(-|x - x'|/\lambda(x')), \quad (5)$$

where $\lambda(x')$ is the local electron mean free path at the position x' .

We have shown in Ref. ^[12] that solving the equation $\partial_x q_{NL}(x) = S$ using this non-local expression for the heat flux computation can lead to discontinuities in the temperature profile if the source term S is very localized in space, such as for example, in the case of the interaction with the wall, and the collisionality takes medium and low values as it can happen in the scrape-off layer (SOL) plasma of tokamaks. In order to overcome this issue we have introduced (see again Ref. ^[12]) the following expression for the heat flux:

$$q_{NL,T}(x) = \widetilde{q_{NL}}(x) + q_{BC,0} \exp\left(-\frac{x}{\lambda}\right) + q_{BC,L_{\parallel}} \exp\left(\frac{x - L_{\parallel}}{\lambda}\right) \quad (6)$$

This expression exhibits a first term describing the non-local heat flux computed from the continuous temperature gradient expression in the plasma. The two last terms represent the impact of the boundary condition in the heat flux, effect that decays exponentially away from the wall. They describe the long range influence of the boundary conditions. The values $q_{bc,0}$ and $q_{bc,L_{\parallel}}$ are adjusted to match the sheath boundary condition for the heat flux, namely $q_{se} = \gamma n_{wall} c_s T_{wall}$ at both ends where γ is the so called sheath transmission coefficient. We note that the value of the sheath heat transmission coefficient gamma depends also on the collisionality of the system and can take very large values when the high-energy tail exists (see for example Ref. ^[13] and ^[14]). However, for steady state condition like the one considered in this paper, the sheath transmission coefficients are quite constant for a large range of collisionality values.

2 Non-local heat transfer in fluid models: Application to 1D Scrape-off layer with localized particle and energy sources

We consider a 1D model of SOL plasma where we solve the standard equations for density, parallel momentum and ion and electron energy balance with standard Bohm boundary conditions, including the non-local expression for heat flux introduced above. Localized sources of density (particle recycling) and energy (e.g. RF heating for both electrons and ions) have been added as follows. For the particle source, simulating a recycling source term we have imposed

$$S_n(x) = S_n^0 \left[\exp\left(-\frac{x}{0.1L_{\parallel}}\right) + \exp\left(-\frac{L_{\parallel} - x}{0.1L_{\parallel}}\right) + 0.005 \right], \quad (7)$$

while for the energy sources, we have used Gaussian shaped sources located at the middle of the field line. The width of the energy source is controlled by λ_E and reads

$$S_{Ee,i} = S_{Ee,i}^0 \exp\left(-\left(\frac{x}{\lambda_E} - \frac{L_{\parallel}}{2\lambda_E}\right)^2\right). \quad (8)$$

We report here two cases obtained varying the amplitude of the energy source and producing a first case at medium collisionality $\nu^* = 60$ and a second one at low collisionality with $\nu^* = 4$ where $\nu^* = L_{\parallel}/\lambda$ with λ the electron mean free path. We note that, for the medium collisionality case (see Fig. 3) the non-local expression collapses onto the standard SH expression with very small contribution coming from the non-local terms related to the influence of the boundary conditions. However, the $q_{e,BC}$ contribution is, as expected, non-negligible very close to the wall, see again the dotted line in Fig. 3. On the contrary, when the collisionality drops, the non-local expression is able to take into account the influence of the boundary conditions on the whole domain. In Fig.4 it appears clear that the contribution from the $q_{e,BC}$ expression to the total parallel heat flux is non-negligible on the entire domain and of the same order of magnitude of the conductive part. Interestingly, thanks to the proposed non-local expression, we can also recover the shape of the energy source into the temperature profile, which is Gaussian in the energy source region (see Fig. 4 panel a).

In next section we introduce the kinetic modeling of heat transfer which will be used for a first analysis of the results obtained in this section.

3 Kinetic modelling of heat transfer

From the kinetic point of view, weakly collisional plasmas are usually studied in terms of their phase-space distribution function $f(\mathbf{r}, \mathbf{v})$ by means of the so-called Vlasov-Fokker-Planck equation (see e.g. ^[15–17]) that reads for the electron

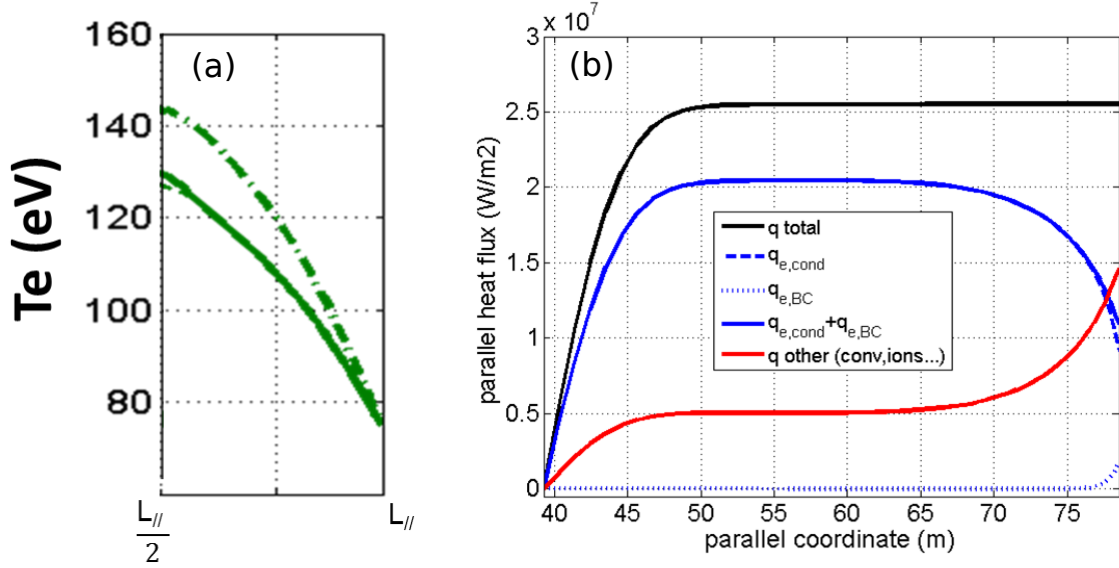


Figure 3: Electron temperature profile along x parallel to magnetic field B from upstream position ($x = 39m$) to the wall ($x = 78m$) obtained from SOLEDGE1D simulation at $\nu^* = 60$. The solid line represents the results obtained considering the non-local heat flux expression, the dashed line using the SH expression and the dashed-dotted line the flux limiter expression with the free parameter $\alpha = 0.15$ (a). Heat flux profile along x parallel to B from upstream position to the wall. The solid blue line is the sum of the contribution from the electron conductive term (reported with dashed line and dominant in this case) and the contribution from the $q_{e,BC}$ expression (see Eq. (6)) represented in dotted line, representing the long-range influence of the boundary conditions and very small in this case apart very closely to the target. The red solid line is the contribution from the remaining extra terms (e.g. convective, ions), while solid black line is the total heat flux (b).

components as

$$\frac{\partial f}{\partial t} + \mathbf{v} \cdot \nabla_{\mathbf{r}} f - \frac{e}{m_e} \left(\mathbf{E} + \frac{\mathbf{v}}{c} \times \mathbf{B} \right) \cdot \nabla_{\mathbf{v}} f = \nabla_{\mathbf{v}} \cdot (\nu \nabla_{\mathbf{v}} f). \quad (9)$$

In the equation above, the diffusion coefficient ν appearing in the velocity-space diffusive term at the rhs could be in principle an explicit function of velocity, or be dependent on position through the local number density $n(\mathbf{r}) = \int f d\mathbf{v}$, see [18, 19].

Equation (9) can be easily integrated with standard implicit Eulerian codes in the 1D1V and 1D2V cases [16], adopting standard Maxwell solvers to account for the self-consistent electric and magnetic fields \mathbf{E} and \mathbf{B} . Already in 2 spatial dimensions (2D2V or 2D3V) such approach rapidly becomes numerically expensive and we therefore rely on particle¹ based (semi-)Lagrangian methods such as particle-in-cell (PIC, see e.g. [20]). Including the contribution of collisions in cell-based PIC codes is usually time consuming and model dependent, here we used a stochastic approach based on the multi-particle collision (hereafter MPC) technique.

¹Note that particles are to be thought as a discrete sampling of f , rather than actual “particles”.

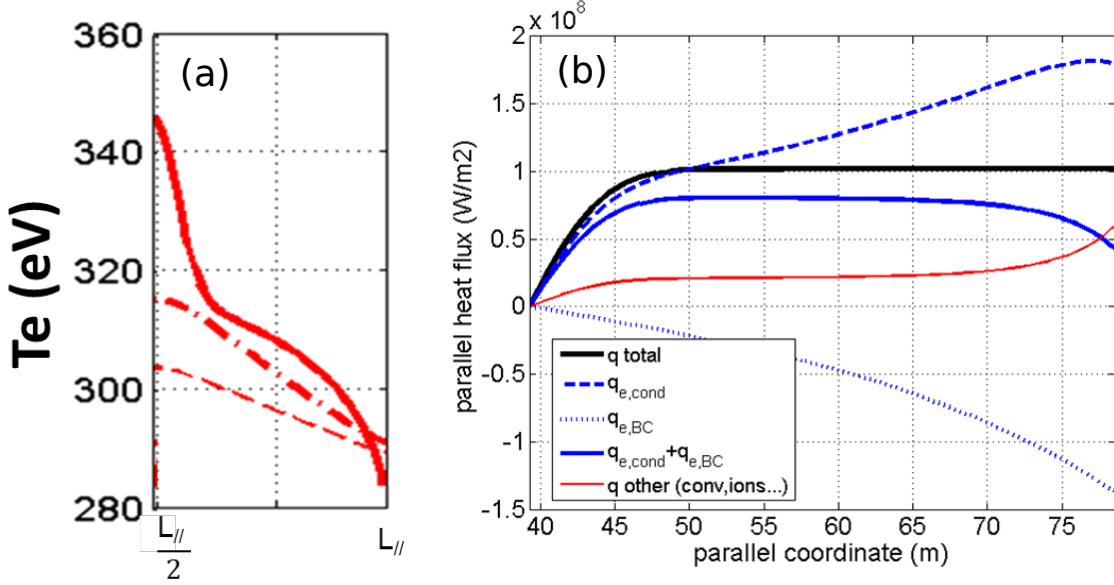


Figure 4: Electron temperature profile along x parallel to magnetic field B from upstream position ($x = 39m$) to the wall ($x = 78m$) obtained from SOLEDGE1D simulation at $\nu^* = 4$. Line types in figures are the same as those in Fig. 3 (a). Heat flux profile along x parallel to B from upstream position to the wall. Line types in figures are the same as those in Fig. 3. In this case the $q_{e,BC}$ contribution (dotted blue line) related to non-local effects is very large (b).

3.1 Multi-particle collision method

Originally introduced by Malevanets and Kapral^[21] for the simulation of complex fluids (e.g. polymers in solution, colloidal fluids), in 3 spatial dimension, the MPC scheme partitions the system of N_p particles in N_c cells². Between two standard propagation steps, inside each cell the particle velocities in the cell's centre of mass $\delta\mathbf{v}_j = \mathbf{v}_j - \mathbf{u}_i$ are rotated of an angle φ around a random axis \mathbf{R} and then converted back to the simulation frame, so that for the j -th particle in cell i

$$\mathbf{v}'_j = \mathbf{u}_i + \delta\mathbf{v}_{j,\perp} \cos(\varphi) + (\delta\mathbf{v}_{j,\perp} \times \mathbf{R}) \sin(\varphi) + \delta\mathbf{v}_{j,\parallel}, \quad (10)$$

where $\delta\mathbf{v}_{j,\perp}$ and $\delta\mathbf{v}_{j,\parallel}$ are the relative velocity components perpendicular and parallel to \mathbf{R} , respectively. Such operation exactly conserves in each cell the total kinetic energy K_i and the three components of the momentum \mathbf{P}_i . For an extensive proof of the conservation laws see Appendix A in^[27]. In addition, it is also possible to conserve the component of the angular momentum \mathbf{L} parallel to \mathbf{R} by choosing φ so that

$$\sin(\varphi) = -\frac{2a_i b_i}{a_i^2 + b_i^2}; \quad \cos(\varphi) = \frac{a_i^2 - b_i^2}{a_i^2 + b_i^2}, \quad (11)$$

²In our implementation the mesh used in the MPC step is the same as the one used by the PIC code to compute electromagnetic fields.

with cell-dependent coefficients a_i and b_i given by

$$a_i = \sum_{j=1}^{N_i} [\mathbf{r}_j \times (\mathbf{v}_j - \mathbf{u}_i)]|_z; \quad b_i = \sum_{j=1}^{N_i} \mathbf{r}_j \cdot (\mathbf{v}_j - \mathbf{u}_i). \quad (12)$$

In the formulae above, \mathbf{r}_j are the particles position vectors, and the notation $|_z$ means that one is taking (without loss of generality) the component of the vector \mathbf{A}_i parallel to the z axis of the simulation's coordinate system.

For two dimensional systems, Equation (10) reduces to $\mathbf{v}'_j = \mathbf{u}_i + \mathbf{G}_{\varphi,i} \cdot \delta \mathbf{v}_j$, where $\mathbf{G}_{\varphi,i}$ is a 2D rotation matrix of an angle φ chosen according to relations (11,12), see Ref.^[27]. In both 2D and 3D cases, the generalization to multi-mass models is straightforward and implies the substitution of velocity vectors with momentum vectors.

In one dimension, the multi-particle collision involves instead a velocity sign inversion with a momentum shift (see also ^[26]) and the two conserved quantities are the linear momentum P_i and the kinetic energy K_i . During the collision step the stochastic momentum shifts w_j are extracted for each particle from a normal distribution depending on the cell temperature, so that the conservation of P_i and K_i now reads

$$\begin{aligned} P_i &= \sum_{j=1}^{N_i} m_j v_j = \sum_{j=1}^{N_i} m_j v'_j = \sum_{j=1}^{N_i} (c_i w_j + d_i m_j); \\ K_i &= \frac{1}{2} \sum_{j=1}^{N_i} m_j v_j^2 = \frac{1}{2} \sum_{j=1}^{N_i} m_j v_j'^2 = \frac{1}{2} \sum_{j=1}^{N_i} m_j (c_i w_j / m_j + d_i)^2, \end{aligned} \quad (13)$$

where N_i is the number of particles in cell i , m_j and v_j are the j -th particles mass and velocity, and c_i and d_i are unknown cell-dependent quantities. Eqs. (13) constitute a linear system that to be solved for c_i and d_i . We define the stochastic momentum and kinetic energy increments

$$P_i^* = \sum_{j=1}^{N_i} w_j; \quad K_i^* = \frac{1}{2} \sum_{j=1}^{N_i} w_j^2 / m_j, \quad (14)$$

and rescale them, together with P_i and E_i , by the total mass in cell i , $M_i = \sum_{j=1}^{N_i} m_j$ as $\tilde{P}_i^* = P_i^* / M_i$, $\tilde{P}_i = P_i / M_i$, $\tilde{K}_i^* = K_i^* / M_i$ and $\tilde{K}_i = K_i / M_i$. The coefficients c_i and d_i are then easily computed as

$$c_i = \sqrt{\frac{2\tilde{K}_i - \tilde{P}_i^2}{2\tilde{K}_i^* - \tilde{P}_i^{*2}}}; \quad d_i = \tilde{P}_i - \tilde{P}_i^* c_i, \quad (15)$$

so that the new velocities after the multi-particle collision finally read $v'_j = c_i w_j / m_j + d_i$.

In a series of papers on the anomalous diffusion and heat transfer in 1D one-component plasmas ^[23, 25–27], we have applied a hybrid PIC-MPC technique where velocity exchange inside the cells is conditioned to an interaction

probability \mathcal{P}_i dependent on the local plasma parameters, in order to account for Coulomb collisions in a more physical way and also to treat spatially and thermally inhomogeneous systems.

In each cell we define the species-averaged *plasma coupling parameter*

$$\bar{\Gamma}_i = \frac{E_{C,i}}{k_B T_i}, \quad (16)$$

where $E_{C,i} = \langle q^2 \rangle_i / 4\pi\epsilon_0 \xi_i$ is the mean Coulomb energy per particle, $\langle q^2 \rangle_i$ the particles average (squared) charge in cell i , and ξ_i is a typical inter-particle distance depending on the local particle number density n_i , finally, the cell temperature T_i is assumed to be proportional to the average kinetic energy of the particles inside the cell as $k_B T_i = (1/N_i) \sum m_j v_j^2$. Before the collision step, the code evaluates for each cell the (multi-particle) collision probability as

$$\mathcal{P}_i = \frac{1}{1 + \bar{\Gamma}_i^{-2}}. \quad (17)$$

After sampling a random number \mathcal{P}_i^* from a uniform distribution in the interval $[0, 1]$, the multi-particle collision happens if $\mathcal{P}_i^* / \mathcal{P}_i \leq 1$.

3.2 Preliminary 1D kinetic simulations

Here we present numerical simulations of 1D systems modelling the plasma dynamics along a field line between a hot thermal bath (upstream region) and the colder wall region. In this preliminary work we always assume regimes of strong correlation between ion and electron motion as well as fulfillment of quasi-neutrality condition. In such conditions, the main contribution to the heat flux is due to electrons (see panels (b) of Figs. 3 and 4), we therefore consider a single component system representing the electrons and treat the ions as a non-interacting background adjusting itself as the electron density n_e evolves, in order to yield a globally null electric field. With such assumptions Equation (9) becomes a standard one dimensional Fokker-Planck equation of the form $\partial_t f + v \partial_r f = \partial_v (\nu \partial_v f)$.

In our PIC-MPC code the interaction with the hot source and the wall is modeled with standard Maxwellian thermal baths. In practice, when a simulation particle enters the hot region its velocity v is substituted with a new velocity v' taken from a Maxwellian distribution at temperature T_{Hot} . when instead the particle hits the cold wall, it is either reflected elastically, or re-immitted in the simulation domain with a velocity taken from a Maxwellian distribution at temperature T_{Cold} , with probabilities one-half. Note that, with such choice, the total particle number N_p is conserved as no particle leaves the system. In principle, it is also possible to account for particle evaporation by considering an additional velocity-dependent exclusion protocol that selects hotter particles and removes them from the system. A "stochastic evaporation" algorithm is currently under testing and will be discussed in a forthcoming

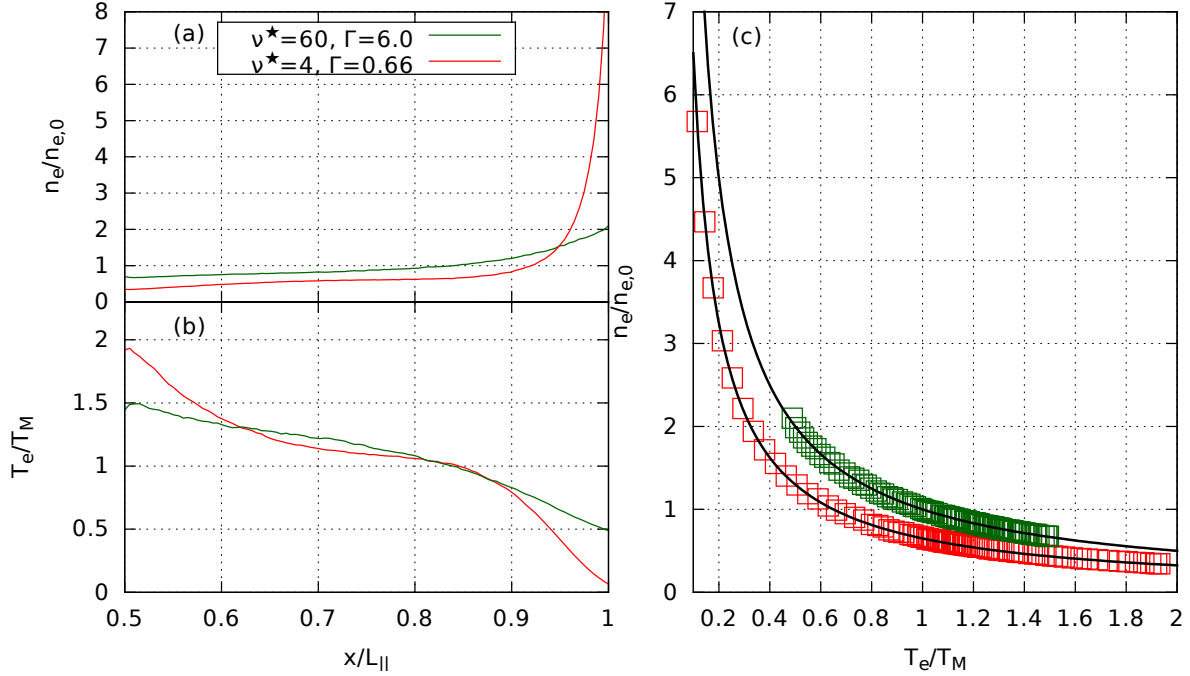


Figure 5: For two models with $\Gamma = 6$ and 0.66 : final electron number density n_e (a) and temperature profile T_e (b) as function of the parallel coordinate $x/L_{||}$, and density temperature relation (squares) and best-fit curves (solid lines), (c). Parallel density and temperature profiles are given only for $L_{||}/2 \leq x \leq L_{||}$, as they are perfectly symmetrical in the other half of the simulation domain.

publication.

Particle propagation is carried out with a standard second order leap-frog scheme while collisions are accounted for as described in Sec. 3.1. All simulations discussed here were performed with fixed timestep $\delta\tau = 0.01\Omega_P^{-1}$, where $\Omega_P = \sqrt{n_e e^2 / m_e \epsilon_0}$ is the plasma frequency of the system neglecting the thermal motion, and extended up to $\tau = 10^3 / \Omega_P$.

In the kinetic simulations we have taken the same combinations of temperature, density and parallel length as in the two cases discussed in Sect. 2, yielding the two values of the collisionality $\nu^* = 60, 4$. We have assumed equilibrium initial conditions by placing the particles representing the electron component homogeneously on the simulation domain $[0, L_{||}]$ (i.e. constant initial electron number density $n_{e,0}$), with velocities taken from a thermal distribution at temperature $T_{e,0}$. After a short transient of about $10\delta\tau$ the thermal baths at $T_{\text{hot}} = 130$ eV and $T_{\text{cold}} = 78$, and $T_{\text{hot}} = 345$ eV and $T_{\text{cold}} = 285$ eV for the $\nu^* = 60$ and $\nu^* = 4$ cases are applied for both cases in $x = L_{||}/2$ and $x = 0, L_{||}$.

From the initial values of the electron temperature and density $T_{e,0}$ and $n_{e,0}$ we derive the initial global plasma coupling parameter $\Gamma = E_{C,0} / k_B T_0$ that gives another measure of how strong is the system's collisionality (at least) in its initial state (i.e., at fixed $L_{||}$ or at fixed Ω_P , larger Γ implies higher collisionality). With the present combination

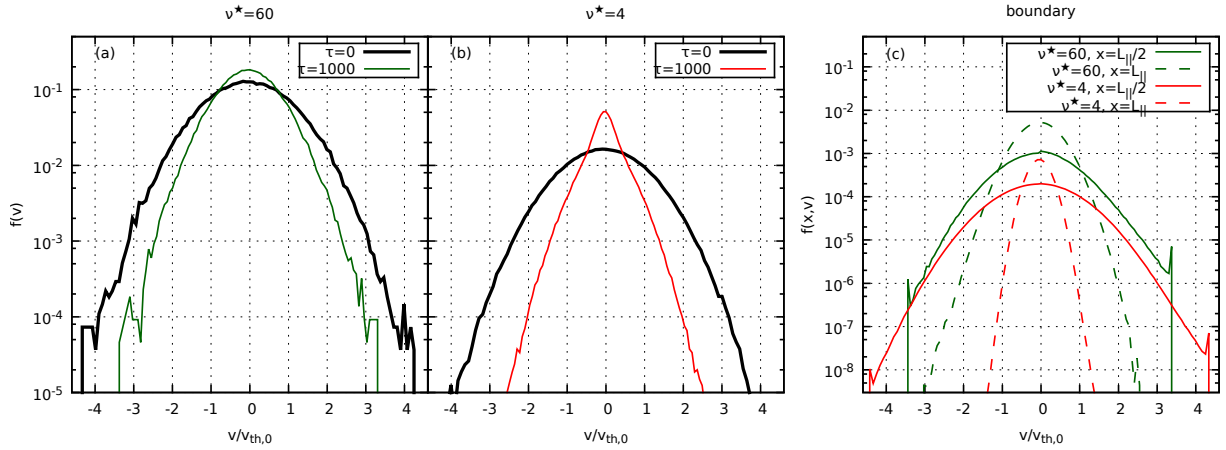


Figure 6: Velocity distributions $f(v)$ for the case with $\nu^* = 60$ (a) and $\nu^* = 4$ (b). The thin solid lines correspond to the equilibrium state (reached at around $\tau \approx 10^3$), while the heavy solid line mark the initial velocity distributions. Sections of the phase-space distribution function $f(x, v)$ at the cold wall (dashed lines) and hot (solid lines) (c). In all cases the velocities are normalized with respect to the initial thermal velocity $v_{th,0}$.

of parameters we obtain $\Gamma \approx 6$ for $\nu^* = 60$ and $\Gamma \approx 0.66$ for $\nu^* = 4$.

Figure 5 shows the asymptotic equilibrium state of the two models with collisionality $\nu^* = 60$ and 4 ($\Gamma = 6$ and 0.66), in contact with a hot source at $x = L_{||}/2$ and a cold wall at $x = 0$ and $L_{||}$. In both cases the systems (consistently) show non-uniform density profiles with a density accumulation in correspondence of the cold source. Vice-versa, the density depletes approaching the hot source, due to the larger mean velocities of particle in this region. At variance with Figs. 3-4, the electron temperature T_e is given in units of the system's mean final temperature T_M , so that the two curves can be more easily compared being on the same scale. The initially more collisional system (i.e. $\Gamma = 6$) has a quasi-linear temperature profile over a broader interval of the parallel coordinate x (i.e. $0.5 \leq x/L_{||} \leq 0.73$), while the weakly collisional system has a more complex asymptotic temperature profile characterized by several slope changes and a flat central region (remarkably similar to the corresponding curve in Fig. 4, panel a), pointing to a highly non-local heat transport regime. Remarkably, in both cases the final electron pressure $P_e \propto n_e T_e$ is spatially constant as we clearly observe $n_e \propto T_e^{-1}$ at $\tau = 10^3$ (panel c).

Figure 6 shows for the same systems of Fig. 5 the initial and final velocity distributions $f(v)$ (panels a, b) and the sections of (half of) the numerically-recovered phase-space distribution function $f(x, v)$ at $x = L_{||}/2$ and $x = L_{||}$ (panel c). The strongly interacting model with $\nu^* = 60$ presents a final $f(v)$ that is well described by a Gaussian, while the model with $\nu^* = 4$ has a clearly non-thermal final velocity distribution. Both cases, however, appear to be colder in their final state with respect to their initial states. For what concerns the phase-space distribution, while in both cases $f(x, v)$ clearly approaches a thermal distribution in correspondence of the cold point, the structure of $f(x, v)$ at $x = L_{||}/2$ is somewhat more complicated and characterized by a fatter tail at positive velocities (i.e. corresponding to particles moving *towards* the cold point). In addition, in correspondence of the highest velocities

attained by the particles, two peak-like structures can be clearly seen. We interpret this feature as a finite-size effect due to the almost vanishing life-time of larger velocities reaching the cold wall. In fact, at fixed ν^* , Γ , and thermal baths temperatures T_{hot} and T_{cold} , such peaks tend to disappear for increasing L_{\parallel} .

4 Conclusion and outlook

We have shown the impact of flux limiter techniques on the computation of heat flux on divertor tokamak simulations. We have proposed the implementation of a non-local approach in a 1D fluid model and we have presented the numerical results obtained with SOLED1D at medium and high collisionality. In the second part of the paper a PIC-MPC kinetic simulations are presented. they offer a particle-based approach that appears to be more suitable to study transient regimes and relaxation processes. Remarkably, for the case studies discussed in this paper, we found good agreement between this approach and the fluid modelling, suggesting that further evolutions of the fluid scheme could be tested against more detailed particle-in-cell-MPC simulations including more species and the effect of the self-consistent fields.

Acknowledgments

This work has been carried out within the framework of the EUROfusion Consortium and has received funding from the Euratom research and training program 2014-2018 under grant agreement No 633053 for the project WP17-ENR-CEA-01. The views and opinions expressed herein do not necessarily reflect those of the European Commission. This work was granted access to the HPC resources of Aix-Marseille University financed by the project Equip@Meso (ANR-10-EQPX-29-01) of the program “Investissements d’Avenir” supervised by the Agence Nationale pour la Recherche. P.F.D.C. acknowledges partial support by the INFN project DYNYSMATH 2017.

References

- [1] H. Bufferand, et al. **2015**, p. 053025., Nuclear Fusion.
- [2] S. Wiesen, et al. **2015**, p. 480., Journal of Nuclear Materials.
- [3] C. Guillemaut, et al **2014**, p. 093012., Nuclear Fusion.
- [4] K. Shimizu, et al **2009**, p. 065028., Nuclear Fusion.
- [5] T. D. Rognlien, et al **1994**, p. 362., Contr. Plasma Phys.
- [6] L. Spitzer, R. Härm, *Physical Review* **1953**, *89*, 977-981, DOI 10.1103/PhysRev.89.977.
- [7] P. Stangeby **2000**, Bristol: Institute of Physics Publishing.

- [8] W. Fundamenski **2005**, p. R163., *Plasma Physics and Controlled Fusion*.
- [9] J. Bucalossi, et al **2014**, p. 907-912., *Fusion Engineering and Design*.
- [10] G. Ciraolo, et al **2017**, p. 187-192., *Nuclear Materials and Energy*.
- [11] A. V. Chankin, et al **2006**, p. 839-868., *Plasma Physics and Contr. Fusion*.
- [12] H. Bufferand, et al **accepted**, *Contribution to Plasma Physics*.
- [13] D. Tskhakaya, et al., *Contributions to Plasma Physics* **2008**, *48*, 89-93, DOI 10.1002/ctpp.200810015.
- [14] A. Froese, T. Takizuka, M. Yagi, *Contributions to Plasma Physics* **2012**, *52*, 534-538, DOI 10.1002/ctpp.201210045.
- [15] K. Dressler, *Mathematical Methods in the Applied Sciences* **1990**, *12*, 471-487.
- [16] E. J. Allen, H. D. Victory, *Physica A Statistical Mechanics and its Applications* **1994**, *209*, 318-346.
- [17] A. R. Bell, et al., *Plasma Physics and Controlled Fusion* **2006**, *48*, R37-R57, DOI 10.1088/0741-3335/48/3/R01.
- [18] M. N. Rosenbluth, W. M. MacDonald, D. L. Judd, *Physical Review* **1957**, *107*, 1-6, DOI 10.1103/PhysRev.107.1.
- [19] W. M. MacDonald, M. N. Rosenbluth, W. Chuck, *Physical Review* **1957**, *107*, 350-353, DOI 10.1103/PhysRev.107.350.
- [20] R. W. Hockney, J. W. Eastwood, *Computer Simulation Using Particles* **1981**.
- [21] A. Malevanets, R. Kapral, *Journal of Computational Physics* **1999**, *110*, 8605-8613.
- [22] H. Noguchi, G. Gompper, *Phys. Rev. E* **2008**, *78(1)*, 016706.
- [23] H. Bufferand, G. Ciraolo, P. Ghendrih, P. Tamain, F. Bagnoli, S. Lepri, R. Livi, One-dimensional particle models for heat transfer analysis, *Journal of Physics Conference Series*, vol. 260 **2010**, 012005.
- [24] J. F. Luciani, P. Mora, J. Virmont **1983**, p. 1665., *Phys. Rev. Lett.*
- [25] H. Bufferand, G. Ciraolo, P. Ghendrih, Lepri S., R. Livi, *Phys. Rev. E* **2013**, *87(2)*, 023102.
- [26] P. Di Cintio, R. Livi, H. Bufferand, G. Ciraolo, S. Lepri, M. J. Straka, *Phys. Rev. E* **2015**, *92(6)*, 062108.
- [27] P. Di Cintio, R. Livi, S. Lepri, G. Ciraolo, *Phys. Rev. E* **2017**, *95(4)*, 043203.

